

provides a reasonable explanation for the observed $C\beta$ spin densities, and that it is important to distinguish s and p populations when estimating hyperfine interactions for the nitrogens. Because of the strong interaction between the two spin subsystems, it may be an oversimplification to label HRP-I as an "a_{2u} cation radical".¹⁴ The differences in π spin populations between the present calculations and earlier ones may not be significant, but the possible

consequences of significant mixing between the FeO and porphyrin spin systems need to be considered when empirical assignments are made. Further studies on these systems, incorporating spin-polarization and spin-orbit effects, are in progress.¹⁵

Registry No. Fe(P)⁰, 32647-22-6; Fe(P)(py)⁰, 60817-63-2; Fe(P)(py)(O)⁰, 96453-16-6; peroxidase, 9003-99-0.

(14) For a recent discussion of the classification of HRP-I, see: Morishima, I.; Takamuki, Y.; Shiro, Y. *J. Am. Chem. Soc.* **1984**, *106*, 7666-7672.

(15) This work was supported in part by grants from NIH and NSF; computer time was provided by California State University, Sacramento.

Substrate Analogue Binding to the Coupled Binuclear Copper Active Site in Tyrosinase

Dean E. Wilcox,[†] Arturo G. Porras,[†] Yeong T. Hwang,[†] Konrad Lerch,[‡] Marjorie E. Winkler,[†] and Edward I. Solomon*[†]

Contribution from the Department of Chemistry, Stanford University, Stanford, California 94305, and Biochemisches Institut, Universitat Zurich, CH-8028 Zurich, Switzerland. Received September 7, 1984

Abstract: Chemical and spectroscopic studies are presented for the binding of a series of carboxylate competitive inhibitors to the oxy ($[2Cu^{II}-O_2^{2-}]$), met ($[2Cu^{II}]$), and half-met ($[Cu^{II}Cu^I]$) derivatives of the binuclear copper active site in tyrosinase. These inhibitors are found to divide into two groups: (1) poor inhibitors, which show an equilibrium constant for binding to the enzyme similar to that for binding to aqueous Cu(II) complexes, and (2) good inhibitors, which are substrate analogues in that the carboxylate is conjugated into an aromatic ring, producing a planar structure and which bind with an equilibrium constant higher by an order of magnitude relative to aqueous copper. Associated with this increased stability are unusual Cu(II) spectral features which relate to a difference in the geometry of substrate binding to the copper site. The poor inhibitors produce normal EPR, absorption, and CD spectral features typical of tetragonal Cu(II) in a square-pyramidal structure with the Cu displaced by ~ 0.3 Å toward the axial ligand. Alternatively, the unusual spectral features associated with good competitive inhibitor binding to the copper site (large rhombic splitting of the g_{\perp} region, large hyperfine splitting of the lowest g value, and a low energy (<10000 cm⁻¹) transition in the CD spectrum) result from a significant distortion of the Cu(II) site toward a trigonal bipyramidal geometry along the C , distortion coordinate for associative ligand substitution reactions of square-planar and tetragonal complexes. A ligand field analysis of this coordinate is presented and used to estimate the geometry of this substrate-bound active site complex. From this analysis, the protein pocket appears to contribute to the stabilization of substrate analogue binding in a geometry which is midway along this reaction coordinate. The contribution of this substrate-protein interaction to the ortho-hydroxylation reaction of oxytyrosinase is discussed, and possible electronic pathways for this reaction are considered, based on the geometric and electronic structure of the spectroscopically effective model for the ternary complex formed by substrate, dioxygen, and the binuclear copper active site.

Tyrosinase contains a coupled binuclear copper site which catalyzes the hydroxylation of monophenols to *o*-diphenols (cresolase activity) and the two-electron oxidation of *o*-diphenols to *o*-quinones (catecholase activity). Isotopic studies have demonstrated that the oxygen atom incorporated into the monophenol during oxidation comes from molecular oxygen.¹ Chemical and spectroscopic studies of tyrosinase have shown that its coupled binuclear copper active site is very similar to that found in the hemocyanins.² This binuclear copper site can be prepared in a variety of forms, and the systematic study³ of these derivatives has greatly added to our understanding of the geometric and electronic structure of this active site.

In the oxygenated form, the spectroscopically effective model of the active site contains two tetragonal Cu(II) ions with nitrogen and oxygen ligation. These coppers are bridged by an endogenous group (phenolate, hydroxide, or alkoxide) which provides antiferromagnetic coupling between them and results in the lack of an EPR signal.⁴ In addition, the exogenous oxygen molecule is bound as peroxide,^{2a} also bridging the coppers in a μ -1,2 geometry.^{2b} Peroxide bound in this mode produces a distinct $O_2^{2-} \rightarrow Cu(II)$ charge-transfer spectrum which can be correlated to the

optical features of the oxy enzyme and includes an extremely intense absorption band centered at 350 nm ($\epsilon = 26000$ M⁻¹ cm⁻¹).³

Mettyrosinase, like the oxy form, contains two tetragonal copper(II) ions antiferromagnetically coupled through an endogenous bridge, but exogenous ligands other than peroxide are bound to the copper site.^{2b,3} This derivative can be converted by addition of peroxide to oxytyrosinase, which in turn decays back to mettyrosinase upon loss of peroxide. The resting form of tyrosinase is found to be a mixture of $\geq 85\%$ met and $\leq 15\%$ oxy.⁴ In addition, a half met derivative can be prepared which contains the two coppers in a mixed valence oxidation state $[Cu^I-Cu^{II}]$ and which is EPR detectable. The EPR and optical spectral features of this form reflect electron delocalization between the coppers

(1) Mason, H. S.; Fowlks, W. B.; Peterson, E. W. *J. Am. Chem. Soc.* **1955**, *77*, 2914-2915.

(2) (a) Eickman, N. C.; Solomon, E. I.; Larrabee, J. A.; Spiro, T. G.; Lerch, K. *J. Am. Chem. Soc.* **1978**, *100*, 6529-6531. (b) Himmelwright, R. S.; Eickman, N. C.; LuBien, C. D.; Lerch, K.; Solomon, E. I. *J. Am. Chem. Soc.* **1980**, *102*, 7339-7344.

(3) Solomon, E. I. In "Copper Proteins"; Spiro, T. G., Ed.; Wiley-Interscience: New York, 1981; Chapter 2.

(4) Jolley, R. L., Jr.; Evans, L. H.; Makino, N.; Mason, H. S. *J. Biol. Chem.* **1974**, *249*, 335-345.

[†]Stanford University.

[‡]Universitat Zurich.

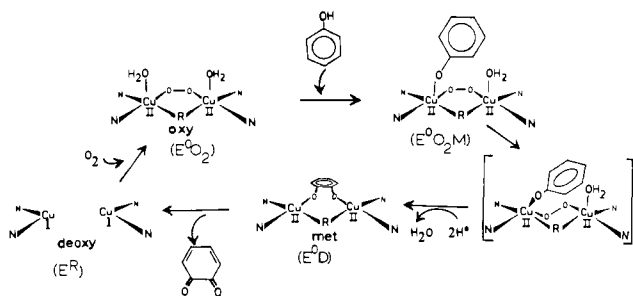


Figure 1. Proposed structural mechanism for oxidative hydroxylation of monophenolic substrates to *o*-quinones by tyrosinase. Adapted from Winkler et al.⁷

and have been found to indicate that exogenous ligands also bridge the two coppers in the half-met derivatives.^{2b,3}

Differences between the tyrosinase and hemocyanin active sites, however, are uncovered by peroxide displacement studies.^{2b,5} Azide displaces the equatorially bound peroxide in an associative displacement mechanism, similar to associative ligand displacement reactions⁶ of square-planar Ni and Pt complexes. These reactions are considered to occur through initial axial coordination by the incoming ligand. This is followed by rearrangement of the five-coordinate complex through a trigonal bipyramidal intermediate with subsequent loss of the displaced ligand. The rates of peroxide placement by azide show that the tyrosinase active site is considerably more accessible to exogenous ligands than the hemocyanin site.^{2b,5}

Mimosine, an analogue of the organic substrate, also displaces peroxide from oxytyrosinase but not from oxyhemocyanin and is found to bind directly to the coupled binuclear copper active site. This is demonstrated by the appearance of a new absorption band at 425 nm, assigned as a phenolate(mimosine)-to-copper(II) charge-transfer transition, upon addition of mimosine to mettyrosinase. Also, addition of mimosine to half-mettyrosinase results in a new, quite unusual EPR signal with large hyperfine splitting of the lowest *g* value. Thus, in tyrosinase, both substrate analogues, and small molecules are capable of binding at the binuclear copper site, with concomitant displacement of peroxide.⁷

Furthermore, ligand competition studies of met- and half-mettyrosinase have shown that the organic substrate analogue (mimosine) and the peroxide analogue (N_3^-) displace each other, competing for the same binding site. Using EPR spectroscopy we have, in fact, observed during this displacement reaction the formation of a ternary intermediate with mimosine and N_3^- simultaneously bound to the half-mettyrosinase active site.⁷

This led to a structural model for the reaction mechanism for ortho-hydroxylation of monophenols and oxidation of the resulting diphenols (Figure 1), which is based on associative ligand substitution at the tyrosinase site. Phenolic substrate initially coordinates to an axial position of one of the coppers of oxytyrosinase. Rearrangement through a trigonal bipyramidal intermediate leads to ortho-hydroxylation by the bound peroxide, loss of H_2O , and coordination of the new diphenol. Subsequent oxidation of the diphenol to a quinone results in a reduced, binuclear cuprous site which releases the quinone and then binds dioxygen to regenerate oxytyrosinase.⁷

To further our understanding of the active site of tyrosinase, we have undertaken a systematic chemical and spectroscopic study of the binding of a series of substrate analogues. Carboxylate ligands were used because they are known competitive inhibitors^{8,9} and because they offer a wide range of structural and electronic variations. We have probed the interaction of substrate analogues

with the binuclear copper site and evaluated the possibilities of substrate interaction with the protein pocket surrounding the copper site. As part of our study, we analyzed the unusual EPR signal associated with substrate analogues bound to half-mettyrosinase and used the spectral features of half-mettyrosinase to probe in detail the geometric and electronic structural features of this active site complex.

Experimental Section

Tyrosinase was obtained from *Neurospora crassa* by the procedure described by Lerch.¹⁰ The purified protein was stored as microcrystals in 10 mM phosphate buffer, pH 7.2, at 4 °C until needed. Samples for experiments were prepared by centrifuging the microcrystals at 27000*g* for 15 min. The supernatant was discarded and the pellet resuspended in a minimum volume of 10 mM phosphate, 1 M NaCl, pH 7.2 solution; this solution was passed through a Sephadex G-25 desalting column, previously equilibrated with the appropriate buffer, to yield the pale yellow mettyrosinase. Tyrosinase solutions were kept on ice to minimize denaturation. Enzymatic activity was measured by the method of Fling et al.¹¹ with L-DOPA as substrate. Aliquots (0.1 mL) of concentrated enzyme were diluted with 2.9 mL of 0.1 M sodium succinate buffer, pH 5.0, containing various concentrations of substrate and inhibitors. To determine the inhibition constants (K_i) of the different carboxylic acids, activity measurements were performed at five inhibitor concentrations, and the data were treated according to Dixon.¹²

Oxytyrosinase for kinetic measurements was prepared by incubating mettyrosinase in 0.1 M potassium phosphate buffer, pH 6.3, with a twofold excess of H_2O_2 for 5 min during which time the pale yellow color of the sample was replaced by the blue color of oxytyrosinase. The solution was then passed through a Sephadex G-25 desalting column previously equilibrated in 0.1 M succinate buffer, pH 5.0. Enzyme thus treated showed an A_{280}/A_{345} ratio of approximately 6, indicating full conversion to oxytyrosinase.⁴ These samples were used immediately, as this form of the enzyme is not stable.

Half-mettyrosinase was prepared by treating 0.5 mM mettyrosinase with 50 mM $NaNO_2$ and 10 mM ascorbate in 0.1 M phosphate buffer, pH 6.3, for 15 min on ice. Excess reagents were removed on a Sephadex G-25 desalting column to provide pure half-met nitrite. Other half-met derivatives were prepared by adding a sufficient amount of the solid ligand to saturate the half-met nitrite solution and allowing the sample to sit 30 min on ice for complete equilibration.

Kinetic studies of peroxide displacement were carried out by adding 0.1 mL of 0.3 mM oxytyrosinase to 1 mL of 10 mM inhibitor solution in a 1.5-mL spectrophotometric cell. Peroxide displacement was monitored at the 345-nm peroxide-to-copper charge-transfer feature on a Cary 17 spectrophotometer equipped with thermostated cell holders maintained at 10 °C by a Lauda/Brinkman RC 20 Model B-2 circulator bath. Benzoic, *p*-bromobenzoic, and acetic acids were obtained from J. T. Baker Chemical Co., *o*-bromobenzoic acid was obtained from Eastman Kodak Co., and picolinic acid was obtained from Reilly Tar and Chemical Co. All other chemicals were obtained from Aldrich Chemical Co. All reagents were used without further purification.

Turnover experiments for both mono- and diphenols were performed by following O_2 consumption during the reactions with an oxygen electrode (Yellow Springs Institute oxygraph).

Absorption spectra were recorded on a Cary 17 spectrophotometer in 1- and 2-cm quartz optical cells at room temperature. CD spectra were taken at room temperature in 1- and 3-cm-pathlength quartz optical cells on a Jasco J-500C spectropolarimeter equipped with a Hammamatsu R-316 phototube. EPR spectra were taken at 77 K on an IBM/Bruker ER-200D spectrometer and recorded on a Nicolet 1180E computer; the microwave frequency for each spectrum was determined with an in-line HP-X532B frequency meter. Subtractions, integrations, and simulations of the EPR spectra were performed on the Nicolet 1180E.

Results and Analysis

1. Thermodynamics and Kinetics. We have measured the binding of a variety of carboxylic acids to oxytyrosinase by following the displacement of peroxide from the coupled binuclear copper active site by using the disappearance of the 345-nm absorption band which corresponds to the $O_2^{2-} \rightarrow Cu(II)$ charge-transfer transition.

After addition of carboxylate to oxytyrosinase, the absorbance at 345 nm decreases slowly in an apparent first-order fashion over

(5) Hepp, A. F.; Himmelwright, R. S.; Eickman, N. C.; Solomon, E. I. *Biochem. Biophys. Res. Commun.* **1979**, *89*, 1050-1057.

(6) Langford, C. H.; Gray, H. B. "Ligand Substitution Processes"; Benjamin; Reading, MA, 1966; Chapter 2.

(7) Winkler, M.; Lerch, K.; Solomon, E. I. *J. Am. Chem. Soc.* **1981**, *103*, 7001-7003.

(8) Duckworth, H. W.; Coleman, J. *J. Biol. Chem.* **1970**, *245*, 1613-1625.

(9) Krueger, R. C. *Arch. Biochem. Biophys.* **1955**, *57*, 52-60.

(10) Lerch, K. *FEBS Lett.* **1976**, *69*, 157-160.

(11) Fling, M.; Horowitz, N. H.; Heinemann, S. F. *J. Biol. Chem.* **1963**, *238*, 2045-2053.

(12) Dixon, M. *Biochem. J.* **1953**, *55*, 170-171.

Table II. Comparison of Binding Constants of Carboxylates to Aqueous Copper and Tyrosinase

	aq Cu	tyrosinase
benzoic acid	40 ^a	800
acetic acid	67 ^a	180
phenylacetic acid	112 ^b	160

^aReference 15; 25 °C, $I = 0.1$. ^bReference 16; 30 °C, $I = 0.1$.

The equilibrium constant for displacement of peroxide from the oxy site by carboxylate was calculated directly from the 345-nm absorbance change observed after no further changes occurred in the oxytyrosinase + carboxylate mixture (~2 h, see Figure 2B). The values obtained are listed in Table I under the heading " K_{disp} ". The main experimental problem associated with obtaining accurate estimates of the equilibrium constants arises from the fact that different preparations of tyrosinase undergo different degrees of conversion to oxytyrosinase. To minimize this variations, simultaneous measurements were taken, in all cases, on several carboxylic acids using aliquots from one batch of enzyme, and a benzoic acid measurement was included as a control. The different data sets were then normalized to each other, and different measurements for the same inhibitor were found to agree with at most 25% variability. This normalization method, then, allowed us to obtain reliable values for the equilibrium (K_{diss}) and subsequently for the kinetic (k_1 , k_{-1} , k_2 , and k_{-2}) constants. Thus, the total errors in our measurements (experimental + fitting errors) are well within the boundaries of $\pm 50\%$ that are usually associated with experiments of the type described in this paper.

Compounds with an aromatic ring conjugated to the carboxylic group where the position ortho to this substituent has been blocked by either a methyl group or a bromine atom (*o*-toluic and *o*-bromobenzoic acids) do not show binding to oxytyrosinase. This phenomenon is specific to substitution at the ortho position and must arise from steric interaction between the protein's active site and the bulky substituent in the ortho position.

The remaining carboxylates show varying abilities to displace peroxide from oxytyrosinase. The equilibrium constant for O_2^{2-} displacement by carboxylate (K_{disp}) are related to the binding constants of the carboxylate to mettyrosinase (K) by the equation

$$K = K_{\text{disp}}/K_{\text{O}_2^{2-}}$$

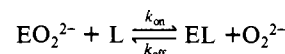
where $K_{\text{O}_2^{2-}}$ is the binding constant for peroxide to mettyrosinase. We have measured the value of $K_{\text{O}_2^{2-}}$ by following the decay of oxytyrosinase (see Figure 2A) and obtained a value of $2 \times 10^4 K_{\text{O}_2^{2-}}$ which is comparable to the value obtained by Mason.⁴ The values of K calculated for the different inhibitors are also listed in Table I.

Examination of the values of K in Table I shows that the organic inhibitors investigated separate into two groups: (1) those showing low binding constants ($K = 150$) and (2) those showing about 1 order of magnitude higher binding affinity ($K = 1000$). The first group comprises inhibitors in which the carboxylic moiety of the molecule is not conjugated into an aromatic system. Other than this structural feature, the nature of the chain attached to the CO_2^- group does not have much effect, as can be seen from comparison of the binding constants for acetic, cyclohexane, carboxylic, and phenylacetic acids. The second group is composed of inhibitors in which the carboxylate is conjugated into an aromatic ring. There is no inductive effect of the substituents on the ring (compare *p*-toluic vs. *p*-bromobenzoic acids) though compounds substituted in the ring position para to the carboxyl seem to bind marginally better to the protein than those with no substituents.

Comparison of the values of K with the stability constants measured for aqueous cupric complexes of carboxylic acids (Table II)^{15,16} shows that there is no significant difference in affinity between aqueous copper and tyrosinase for carboxylates in the nonconjugated group (e.g., phenyl acetate), while there is an order

of magnitude increase in the affinity for the conjugated group (e.g., *p*-toluic acid). This difference cannot be attributed to electronic effects arising from conjugation of the carboxylic group into the aromatic ring (compare $\text{p}K_a = 4.37$ for *p*-toluic acid, and $\text{p}K_a = 4.3$ for phenylacetic acid).¹⁷ Thus, the protein pocket must contribute to the stability of binding of the conjugated ligands by interacting with the planar aromatic portion of the molecule. We have converted the binding affinities of phenylacetic and *p*-toluic acids to binding energies by use of the Arrhenius relation $\Delta G = RT \ln K$ and can estimate a contribution of -2.9 kcal/mol for the carboxylate binding to the binuclear cupric unit and an additional -1.3 kcal/mol for the protein pocket's interaction with the aromatic side chain of *p*-toluic acid.

Knowledge of the rate constant for displacement of peroxide by carboxylate (k_{on}) allows us to calculate the rate for the reverse reaction (k_{off})



k_{off} is then given by $k_{\text{off}} = k_{\text{on}}/K_{\text{disp}}$. The values of k_{off} obtained for the various inhibitors are listed in Table I.

It should be noted that the values of k_{off} in Table I hold remarkably constant throughout the series of carboxylates, so that most of the variation in binding constant (K) can be attributed to changes in the value of k_{on} .

Benzoic acid shows competitive inhibition with respect to the organic substrate in the steady-state measurements of the oxidation of L-DOPA.⁸ To establish a correlation between the affinities for carboxylates measured by displacement of peroxide and affinities under catalytic conditions, we measured the inhibition constants of the carboxylates in Table I during the steady state oxidation of L-DOPA to dopaquinone by molecular oxygen. The reciprocals of the K_1 's are listed in Table I. These values show a reasonable correspondence to the K values for carboxylate binding to mettyrosinase obtained directly from displacement of peroxide from oxytyrosinase. This lends support to the use of these inhibitors as probes of substrate binding to the active site of the protein. All the carboxylic acids investigated were found to give competitive inhibition with respect to L-DOPA, in agreement with the results for benzoic acid previously reported.

The steady-state kinetic behavior of tyrosinase has been used to invoke the presence of at least two different active sites in the enzyme.^{4,8,18} In particular, it has been suggested that the inhibitory patterns of benzoic acid and cyanide on the oxidation of L-DOPA by molecular oxygen indicate the presence of two separate binding sites for the two different substrates.^{8,18} Also the fact that the lag phase in the reaction curve for the oxidation of L-tyrosinase is suppressed by addition of L-DOPA other catechols or hydrogen peroxide and the fact that L-tyrosine interferes with the lag-suppression effect of L-DOPA have been taken to indicate that there are regulatory binding sites in the enzyme which accept these substrates and allow control of the protein's activity in a synergistic fashion.^{4,8} In contrast, Figure 1 requires that all the interactions between tyrosinase and substrates take place at the binuclear Cu site. We have examined the implications of Figure 1 toward the steady-state kinetic behavior of the enzyme and compared this analysis with the literature results.

The inhibitory patterns of benzoic acid, cyanide, and azide have been investigated by various authors for both the monophenolase and diphenolase activities of the enzyme.^{8,18,19} Their results are summarized in Table III. We have examined the kinetic expression associated with all the possible ways an inhibitor could interact with tyrosinase in the context of the reaction pathways presented in Figure 1 and isolated those schemes which are consistent with Table III. The two different types of substrates are found to react with different oxidation states of the coupled

(17) Serjeant, E. P.; Dempsey, B. "Ionisation Constants of Organic Acids in Aqueous Solution"; Pergamon Press: New York, 1979; IUPAC Chemical Data Series No. 23.

(18) Pomerantz, S. H. *J. Biol. Chem.* **1960**, *241*, 161-168.

(19) Healey, D. F.; Strothkamp, K. G. *Arch. Biochem. Biophys.* **1981**, *211*, 86-91.

(15) Martell, A. E.; Smith, R. M. "Critical Stability Constants"; Plenum Press: New York, 1977; Vol. 3.

(16) Ramamoorthy, S.; Santappa, M. *J. Inorg. Nucl. Chem.* **1968**, *30*, 2393-2402.

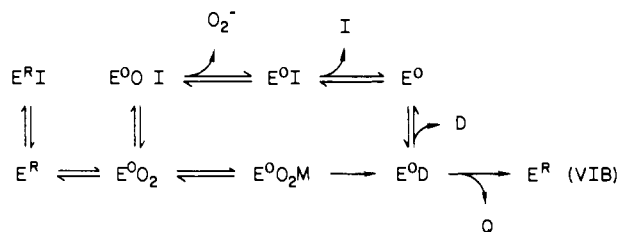
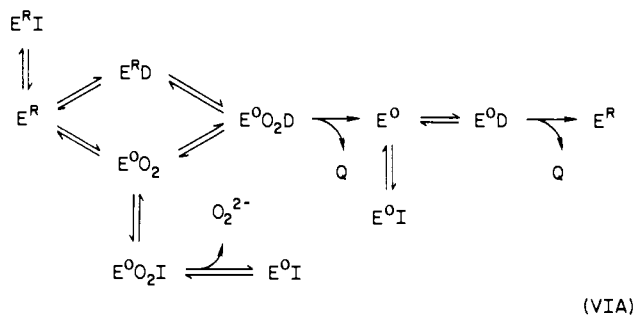
Table III. Inhibition Patterns for Various Inhibitors of Tyrosinase

inhibitor	cresolase activity with respect to		catecholase activity with respect to	
	L-tyrosine	O ₂	L-DOPA	O ₂
carboxylate ^a	competitive	noncompetitive	competitive	noncompetitive
CN ⁻	noncompetitive ^b	noncompetitive	noncompetitive ^a	competitive ^a
N ₃ ^{-c}	noncompetitive	noncompetitive	noncompetitive	noncompetitive

^aReference 8. ^bReference 18. ^cReference 19.

binuclear copper sites. Monophenolic substrates can only react with oxytyrosinase (E⁰O₂) in an ordered sequential mechanism, while diphenolic substrates must also react with mettyrosinase. In addition, these diphenol substrates are required to bind to deoxytyrosinase (E^R), presenting a random sequential mechanism for oxidation of the first molecule of substrate by this oxidation state of the enzyme. This is based on the finding of Duckworth and Coleman⁸ that the nature of the diphenolic substrate can affect the proteins' affinity (K_s) for O₂.

If benzoic acid is treated as an analogue of the organic substrate, competing directly with it for the available forms of the enzyme, the following schemes are appropriate:



where I = inhibitor, M = monophenol, D = diphenol, and Q = quinone. These inhibitory schemes yield the kinetic equations

$$v = k[D][O_2][E]_T / k''(1 + K_1[I]) + k'''[D] + k^{IV}(1 + K_{II}[I])(1 + K_{III}[I])[O_2] + k^V[D][O_2]$$

and

$$v = \frac{k[M][O_2][E]_T}{k''(1 + K_1[I]) + k'''[O_2](1 + K_{II}[I]) + k^{IV}[M][O_2]}$$

for diphenolase and monophenolase activities respectively.

When plotted as double-reciprocal plots (1/v vs. 1/[D] or 1/[M]) for various concentrations of inhibitor (I), the solutions to these equations give the patterns observed experimentally (see Table III). Benzoate is seen to bind to the same forms of tyrosinase as diphenolic substrate (E^R, E⁰O₂, and E⁰) which is what is expected of a substrate analogue.²⁰

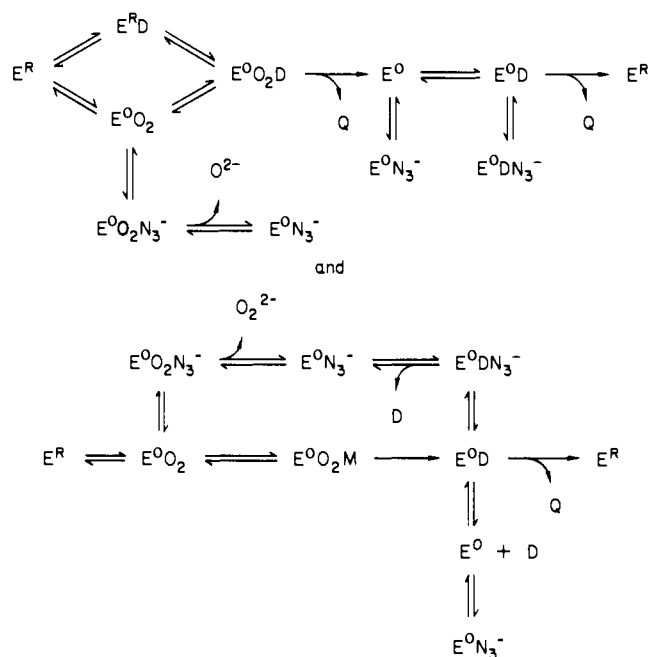
In the case of CN⁻, this molecule is known to bind with high affinity to Cu(I) and stabilize it.²¹ Therefore, if we consider that this molecule inhibits by binding to those forms of the enzyme

in which the binuclear copper site is reduced (E^RD in eq VIA), we find that for the oxidation of L-DOPA

$$v = \frac{k[D][O_2][E]_T}{k'' + k'''[D] + k^{IV}(1 + K_1[I])(1 + K_{III}[I])[O_2] + k^V[D][O_2]}$$

A double-reciprocal plot of the solution to this equation yields patterns which are competitive with varying O₂ and noncompetitive with varying L-DOPA, in agreement with experiment¹⁹ (cf. Table III).

For azide, in turn, Himmelwright et al.³ have shown that it binds to the oxidized forms of the enzyme (E⁰ and E⁰O₂), displacing peroxide in the oxygenated form



which yield the kinetic equations

$$v = k[D][O_2][E]_T / (k'' + k'''[D] + k^{IV}(1 + K_1[I])(1 + K_{II}[I])[O_2] + k^V(1 + K_{III}[I])[D][O_2])$$

and

$$v = k[M][O_2][E]_T / (k'' + k'''[O_2](1 + K_1[I]) + k^{IV}[M][O_2](1 + K_{II}[I])(1 + K_{III}[I]))$$

which when plotted in the double-reciprocal form yield noncompetitive patterns in all cases, in agreement with experimental results.¹⁹

Finally, the lag phase observed during oxidation of monophenol substrates⁸ can be interpreted as simply arising from the decay of oxytyrosinase to mettyrosinase, which is capable of reacting with monophenol substrate, as well as from the dissociation of the enzyme-diphenol complex (E⁰D) which also generates mettyrosinase. Thus, at the beginning of the cresolase reaction under steady-state conditions, only a fraction of the total activity possible is observed. Addition of diphenols or H₂O₂ abolishes the lag phase because these substrates are capable of generating deoxy- and oxytyrosinase, respectively, both of which can turn over, oxidizing monophenol substrate. Monophenol will of course compete with diphenol for binding to the copper site of mettyrosinase, preventing

(20) It should be noticed that benzoate shows similar inhibition patterns for the two different types of substrates in spite of their dissimilar reaction mechanisms. This results because the two main differences (two substrate molecules/turnover cycle for diphenol vs. one for monophenol, and random vs. ordered mechanisms, respectively) combine in a complicated fashion to yield the same inhibition patterns.

(21) Cotton, F. A.; Wilkinson, G. "Advanced Inorganic Chemistry", 4th ed.; Wiley: New York, 1980.

Table IV. Comparison of Kinetic Constants for the Steady-State Oxidation of a Variety of Mono- and Diphenolic Substrates

substrate	K_M , mM	k_{cat} , s ⁻¹
Monophenols		
L-tyrosine	0.59	320
D-tyrosine	0.32	160
tyramine	0.67	160
4-hydroxyphenylacetic acid	0.18	250
<i>p</i> - <i>tert</i> -butylphenol	0.17	1.5
Diphenols		
L-DOPA	1.04	1070
D-DOPA	0.38	340
3-hydroxytyramine	0.28	1350
3,4-dihydroxyphenylacetic acid	4.4	850
<i>p</i> - <i>tert</i> -butylcatechol	1.2	1850

it from turning over to deoxytyrosinase but being unable to react further, so that ever higher levels of diphenol are needed to compete effectively with increased levels of monophenol in the reaction mixture. Even in the absence of added diphenols, the activity of the enzyme reaches its full potential because the product of the four-electron oxidation of tyrosine, dopaquinone, rearranges internally to yield the diphenol leucodopachrome,²² which can react with mettyrosinase, converting it to the deoxy form.

In summary, the various kinetic phenomena observed arise from the mechanistic needs of the reactions catalyzed by tyrosinase. In particular, the hydroxylation of monophenol demands that this substrate react only with oxytyrosinase, giving rise to an ordered sequential mechanism, while the diphenol is free to bind to the oxy, deoxy, and met forms of the enzyme, producing a random sequential mechanism. These, in combination with the individual characteristics of the different inhibitors, give rise to the observed inhibition patterns. Specifically, benzoate behaves as an analogue of diphenol substrate, binding to both oxidized and reduced forms of the coupled binuclear copper site while cyanide binds to the reduced copper site and azide binds to the oxidized copper site. In addition, the dissociability of the diphenol intermediate in the monophenolase reaction (see Figure 1) lends the enzyme some flexibility in its choice of products and, together with decay of oxy- to mettyrosinase, gives rise to the observed lag phase in the monophenolase reaction. It should be emphasized that the kinetic phenomena described arise naturally from the interactions of substrates and inhibitors with the binuclear copper site, and there is no need to invoke allosteric interactions between substrates binding at different sites.

A structural requirement imposed on the monophenol substrate by the mechanism presented in Figure 1 is the ability to rearrange during hydroxylation from an axial toward an equatorial position in the coordination shell of the coppers. In an effort to probe these requirements, we have investigated the effect of changes in the side chain on the activity of the monophenol substrate. The results are given in Table IV. We found little effect of modifying the side chain on the aromatic ring, except for a drastic decrease in the activity of *p*-*tert*-butylphenol as compared with the other substrates. The bulky substituent in this compound would present a barrier to rearrangement of the substrate in the protein pocket. We also ran a parallel series of measurements with the corresponding diphenol substrates (Table IV). The steric requirements on electron transfer to the diphenol are less clear, since no similar "bulky" substituent effect is observed. It is probable that diphenolic substrates need not undergo rearrangement at the Cu site for simple electron transfer.

2. Spectroscopy. A series of half-met carboxylates has been prepared in order to use the EPR signals of this derivative as a higher resolution probe of the structural and electronic features of competitive inhibitor binding to the tyrosinase site. Analogous to the thermodynamic and kinetic results for mettyrosinase in section 1, the carboxylates fall into groups based on the extent of conversion upon their addition to half-met nitrite (see Experimental Section). Ortho-substituted benzoic acid derivatives

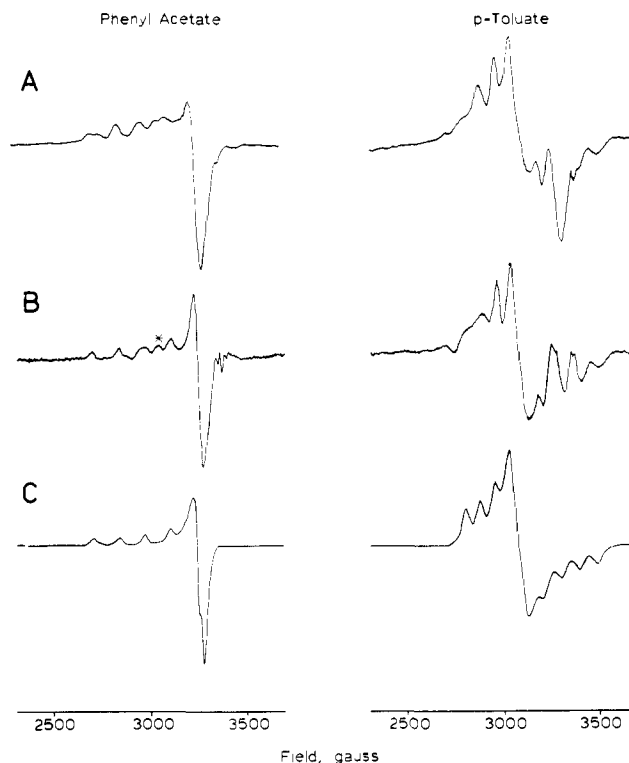


Figure 3. EPR spectra of carboxylate inhibitor complexes with half-mettyrosinase: (A) spectra of carboxylate inhibitors +0.3 mM half-met nitrite in 0.1 M phosphate buffer, pH 6.3 at 77 K; spectral conditions were 9.43-GHz frequency, 10-G field modulation, 10-mW microwave power. (B) Experimental spectra after subtraction of the residual half-met NO₂ signal. The feature labeled * arises from an impurity not present in half-met NO₂ and could not be subtracted out. (C) Simulations of half-met carboxylate signals calculated as described in the text.

Table V. EPR Simulation Parameters for Half-mettyrosinase

	g	$A, \times 10^4 \text{ cm}^{-1}$	line width, G
Phenylacetate			
1	2.080 ± 0.005	0 ± 5	20
2	2.080 ± 0.005	0 ± 5	20
3	2.332 ± 0.005	158 ± 2	20
<i>p</i> -Toluate			
1	2.014 ± 0.005	83 ± 6	25
2	2.195 ± 0.010	22 ± 4	30
3	2.315 ± 0.005	90 ± 2	30

show no conversion and apparently are unable to displace the NO₂⁻. Acetate and phenylacetate, members of the group of poor competitive inhibitors, show low conversion from half-met nitrite while the good inhibitors, benzoic acid, *p*-toluic acid, and *p*-bromobenzoic acid, show higher conversion.

Quantitatively, the extent of conversion is determined by comparing the doubly integrated EPR signal intensities of the half-met carboxylate spectrum, after subtraction of the residual half-met nitrite features, and the initial half-met nitrite spectrum. Correcting for solubility differences, the ratio of the half-met binding affinities for *p*-toluic acid and phenylacetate is determined to be 13, which is comparable to the ratio (12.0) of their binding constants to mettyrosinase (Table I). Therefore, the factors which lead to the high affinity for good inhibitors in mettyrosinase are also present in the half-met derivative.

The half-mettyrosinase EPR spectra with poor and good carboxylate inhibitors also fall into two distinct types. Figure 3 shows (A) the experimental spectra obtained upon addition of phenylacetate and *p*-toluic acid to half-met nitrite, (B) these spectra after subtraction of the residual half-met nitrite features, and (C) the best fit simulations of spectra B; Table V lists the parameters of the best fit simulations. Poor carboxylate inhibitors, represented by phenylacetate, exhibit axial g and $|A|$ ²³ values typical of tet-

(22) Metzler, D. E. "Biochemistry"; Academic Press: New York, 1977.

Table VI. EPR Parameters^a of Representative Five-Coordinate Cu(II) Complexes

	g_1	A_1	g_2	A_2	g_3	A_3
C_{4v} (tetragonal)						
$K[Cu(NH_3)_5](PF_6)_3$ ^b	2.052	(-)21	2.052	(-)21	2.264	(-)182
$[Cu(benzac)_2(EtOH)]$ ^c	2.053		2.053		2.240	
D_{3h} (trigonal bipyramidal)						
$[Cu(tren)(NH_3)](ClO_4)_2$ ^b	2.029	84	2.176	110	2.176	110
$[Cu(NH_3)_2][Ag(SCN)_3]$ ^d	2.006		2.202		2.202	
C_{2v} (intermediate) ^e						
$[Cu(phen)_2(H_2O)](NO_3)_2$ ^f	2.022		2.125		2.227	
$[Cu(bipy)_2H_2O](S_2O_8)$ ^g	2.011		2.158		2.225	
C_s (intermediate)						
$[Cu(Me\ sal)]$ ^h	2.02	47	2.13	65	2.25	131
$[Cu(dien)(bipyam)](NO_3)_2$ ⁱ	2.026	43	2.110	66	2.220	149

^a g and A values from single crystal measurements; A values ($\times 10^4$ cm⁻¹) for complexes doped into isomorphous Zn(II) complexes. ^b Reference 29. ^c Belford, R. L.; Duan, D. C. *J. Magn. Reson.* **1978**, *29*, 293–307. ^d Slade, R. C.; Tomlinson, A. A. G.; Hathaway, B. J.; Billing, D. E. *J. Chem. Soc. A* **1968**, 61–63. ^e A values for magnetically dilute, structurally characterized C_{2v} Cu(II) complexes with N and O ligands apparently have not been determined; Cu(II) doped $[Zn(Me\ saldpt)]$ has a coordination geometry near C_{2v} and shows³⁰ $g_1 = 2.04$, $A_1 = 66 \times 10^{-4}$ cm⁻¹; $g_2 = 2.07$, $A_2 = 38 \times 10^{-4}$ cm⁻¹; $g_3 = 2.23$, $A_3 = 150 \times 10^{-4}$ cm⁻¹. ^f Bencini, A.; Gatteschi, D. *Inorg. Chem.* **1977**, *16*, 1994–1997. ^g Harrison, W. D.; Hathaway, B. J. *Acta Crystallogr., Sect. B* **1979**, *B35*, 2910–2913. ^h Reference 30. ⁱ Ray, N.; Hathaway, B. J. *Chem. Soc., Dalton Trans.* **1980**, 1105–1111.

ragonal Cu(II) complexes with N and O donor ligands. Good carboxylate inhibitors, represented by *p*-toluate, however, show²⁴ a large rhombic splitting of their g values with the lowest value (g_1) near 2.00. Further, significant copper nuclear hyperfine is associated with the lower g values.

Spectroscopic data for half-metmethocyanin^{25,27,28} and tyrosinase³ indicate that the ligand field around the cupric copper is best described as five-coordinate tetragonal with an axially bound exchangeable water. Therefore, it is appropriate to compare the protein's spectroscopic features to those of structurally characterized five-coordinate Cu(II) complexes with N and O donor ligands. Table VI lists the g and $|A|$ values for appropriate analogues representative of four effective symmetry types. Tetragonal, square-pyramidal (C_{4v} , effective symmetry) complexes generally possess a $d_{x^2-y^2}$ ground state which gives rise to $g_{\parallel} > g_{\perp} > 2.00$ and $|A_{\parallel}| > |A_{\perp}|$. Structurally, these model complexes show that as the length of the Cu–L(axial) bond decreases, the Cu(II) is displaced out of the equatorial ligand plane toward this axial ligand. Trigonal bipyramidal (D_{3h} , effective symmetry) complexes have a d_{z^2} ground state, leading to $g_{\perp} > g_{\parallel} = 2.00$ and $|A_{\perp}|, |A_{\parallel}| > 0$. Two lower symmetries, C_{2v} and C_s , which are subgroups common to both C_{4v} and D_{3h} , are also considered for five-coordinate cupric complexes. In C_{2v} site symmetry, a mixed ground state ($\alpha d_{x^2-y^2} + (1 - \alpha^2)^{1/2} d_{z^2}$) is allowed by symmetry and results in a rhombic splitting of the g values, $g_1 \neq g_2 \neq g_3 > 2.00$, and $|A_1|, |A_2|, |A_3| > 0$. C_s site symmetry also allows a mixed ground state ($\alpha d_{x^2-y^2} + b d_{z^2} + c d_{xy}$; $a^2 + b^2 + c^2 = 1$), giving rise to similar g and $|A|$ value relationships.

When the EPR parameters of these model complexes (Table IV) are compared with those of the two half-met carboxylate groups (Table V), the phenylacetate spectrum is readily assigned to a tetragonal (C_{4v}) Cu(II) site symmetry. The rhombic g values and large $|A_{\parallel}|$ value for *p*-toluate, however, place it with a C_{2v} , C_s , or lower effective Cu(II) symmetry.

(23) Note: experimental EPR spectra of frozen solutions give the magnitude, but not the sign, of the hyperfine coupling parameter.

(24) This spectrum cannot be interpreted as a delocalized signal with hyperfine contributions from both Cu nuclei in this mixed-valent site. Half-metmethocyanin forms (see ref 25), which show a delocalized type of EPR spectrum, also have an intense low-energy (near-IR) intervalence transfer (IT) transition associated with the class II mixed-valence electronic structure (see ref 26). Low-temperature (77 K) near-IR optical spectra of half-met-tyrosinase *p*-toluate (saturated sucrose glass), however, show no evidence for such an IT transition. The half-met-tyrosinase carboxylates should therefore be described as localized class I mixed-valence sites, with spectral features arising only from the cupric ion.

(25) Himmelwright, R. S.; Eickman, N. C.; Solomon, E. I. *J. Am. Chem. Soc.* **1979**, *101*, 1576–1586.

(26) Robin, M. B.; Day, P. *Adv. Inorg. Chem. Radiochem.* **1967**, *10*, 247–422.

(27) Himmelwright, R. S.; Eickman, N. C.; LuBien, C. D.; Solomon, E. I. *J. Am. Chem. Soc.* **1980**, *102*, 5378–5388.

(28) Wilcox, D. E.; Mims, W. B.; Solomon, E. I., unpublished results.

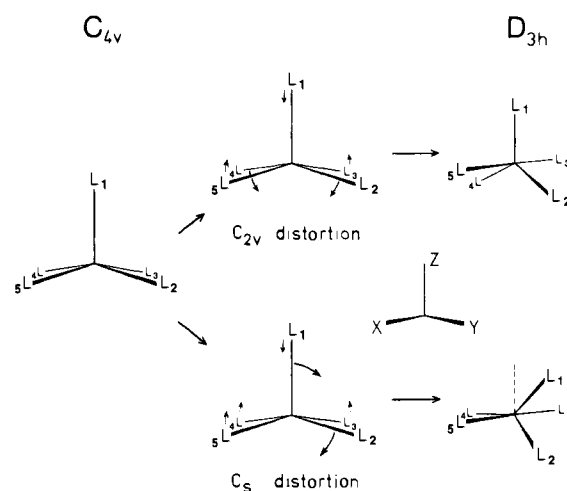


Figure 4. Schematic representation of the C_{2v} (Berry pseudorotation) and C_s structural distortions between tetragonal C_{4v} and trigonal bipyramidal D_{3h} geometries.

The two lower symmetry subgroups common to C_{4v} and D_{3h} are associated with the two structural distortion pathways between these higher symmetries as shown in Figure 4. The more widely studied Berry pseudorotation³¹ coordinate retains an effective C_{2v} site symmetry throughout, and L_2 and L_4 are the "actively distorting" ligands. The second distortion coordinate retains only a mirror plane (C_s effective site symmetry) between the two limiting higher symmetries as L_1 and L_2 are now the actively distorting ligands. This lower symmetry pathway is more difficult to parameterize; however, it is directly related to the reaction coordinate for associative ligand substitution (L_1 displacing L_2 in Figure 4) in square-planar complexes.⁶ For this reason, the C_s distortion coordinate is appropriate for the half-met active site and is considered in more detail.

The structural parameters of the C_s distortion (see Figure 4), starting from the strong square-pyramidal (Cu out of the equatorial plane) limit, are as follows: (a) the axial Cu– L_1 bond shortens and tilts toward L_2 relative to the normal of the plane defined by L_3 , L_4 , and L_5 ; (b) two trans equatorial bonds, Cu– L_3 and Cu– L_5 , shorten and tilt up toward a collinear geometry; (c) the Cu– L_2 bond lengthens and tilts down in the plane defined by L_1 , L_4 , and the Cu (L_2 is the other actively distorting ligand); (d)

(29) Duggan, M.; Ray, N.; Hathaway, B.; Tomlinson, G.; Brint, P.; Pelin, K. *J. Chem. Soc. Dalton* **1980**, 1342–1348.

(30) Bencini, A.; Bertini, I.; Gatteschi, D.; Scozzafava, A. *Inorg. Chem.* **1978**, *17*, 3194–3197.

(31) Berry, R. S. *J. Chem. Phys.* **1960**, *32*, 933–938.

Table VII. Structural Features of Cu(II) Complexes^a Along the C_s Distortion Coordinate

	complexes ^d							
	(C_{4v} limit) A	B	C	D	E	F	G	(D_{3h} limit) H
	Angles, deg							
L_3 -Cu- L_5 ^b	165	167	169	174	176	176	178	180
L_1 -Cu- L_2	98	86	96	101	101	108	113	119.2
L_2 -Cu- L_4	164	165	153	148	146	130	130	119.2
L_4 -Cu- L_1	98	107	112	112	113	122	114	119.2
axial tilt ^c	0	11	17	19	23	30	23	30
	Bond Lengths, Å							
Cu- L_1 (axial)	2.19	2.26	2.17	2.17	2.16	2.11	2.14	2.08
Cu- L_2, L_4 (av)	2.01	1.98	2.02	2.04	2.04	2.06	2.06	2.08
Cu- L_3, L_5 (av)	2.05	1.93	2.02	1.98	1.99	1.97	1.99	2.03

^aSee Figure 4 for ligand assignment. ^bStructural parameter chosen to define the coordinate (see text). ^cSee ref 32. ^dThe complexes are as follows: (A) $K[Cu(NH_3)_5](PF_6)_3$, ref 29; (B) $[Cu(Tsgly)(H_2O)_3]$ (Antolini, L.; Battaglia, L. P.; Battistuzzi Gavioli, G.; Bonamartini Corradi, A.; Grandi, G.; Marcotrigiano, G.; Menabue, L.; Pellacani, G. C. *J. Am. Chem. Soc.* **1983**, *105*, 4327-4332); (C) $[Cu(dien)(HCO_2)](HCO_2)$ (Davey, G.; Stephens, F. S. *J. Chem. Soc. A* **1971**, 103-106); (D) $[Cu(bipy)_2(CH_3CO_2)](ClO_4)(H_2O)$ (Hathaway, B. J.; Ray, N.; Kennedy, D.; O'Brien, N.; Murphy, B. *Acta Crystallogr., Sect. B* **1980**, *B36*, 1371-1377); (E) $[Cu(bipy)_2(HCO_2)](BF_4)1/2(H_2O)$ (Fitzgerald, W.; Hathaway, B. J. *J. Chem. Soc., Dalton Trans.* **1981**, 567-573); (F) $[Cu(bipy)_2(NH_3)](BF_4)_2$ (Stephens, F. S.; *J. Chem. Soc., Dalton Trans.* **1972**, 1350-1352); (G) $[Cu(tren)(NCS)](NCS)$ (Jain, P. C.; Lingafelter, E. C. *J. Am. Chem. Soc.* **1967**, *89*, 6131-6136); (H) $[Cu(tren)(NH_3)](ClO_4)_2$, ref 29.

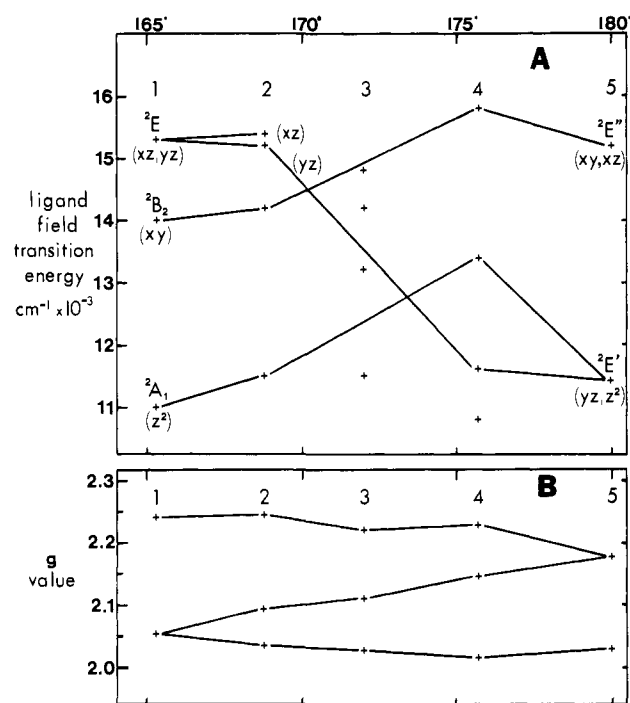


Figure 5. (A) Ligand field transition energies and (B) g values of Cu(II) complexes along the C_s distortion coordinate defined by the L_3 -Cu- L_5 angle (top, see text and Figure 4). Complexes: (1) $K[Cu(NH_3)_5](PF_6)_3$ (A in Table VII), ref 29; (2) $[Cu(dien)(HCO_2)](HCO_2)$ (C in Table VII) (Bew, M. J.; Dudley, R. J.; Fereday, R. J.; Hathaway, B. J.; Slade, R. C. *J. Chem. Soc. A* **1971**, 1437-1441); (3) $[Cu(dien)(bipyam)](NO_3)_2$ (Ray, N.; Hathaway, B. J. *J. Chem. Soc., Dalton Trans.* **1980**, 1105-1111) (ligand field transitions are unassigned due to ambiguous experimental polarizations); (4) $[Cu(bipy)_2(NH_3)](BF_4)_2$ (F in Table VII) (Dudley, R. J.; Hathaway, B. J.; Hodgson, P. G.; Power, P. C.; Loose, D. J. *J. Chem. Soc., Dalton Trans.* **1974**, 1005-1009) (ligand field transitions have been reassigned in the coordinate system of this study; $\psi(d_{xz}) \leftarrow \psi(g_s)$ is forbidden; weak feature at 10800 cm^{-1} is unassigned due to small mixing of experimental polarizations); (5) $[Cu(tren)(NH_3)](ClO_4)_2$ (H in Table VII), ref 28.

the Cu- L_4 bond lengthens and tilts up synchronously with Cu- L_3 and Cu- L_5 . The Cu, L_1 , L_2 , and L_4 plane is retained throughout this coordinate and becomes the trigonal plane of the D_{3h} limit. The C_s distortion coordinate can be quantified by the L_3 -Cu- L_5 angle;³² in the tetragonal limit, this parameter depends on the

degree of displacement of the Cu from the equatorial plane (this also reflects the strength of the Cu- L (axial) interaction) and is typically $\sim 165^\circ$. In the trigonal bipyramidal limit this angle is 180° .

Many five-coordinate Cu(II) complexes (several with bi- or tridentate ligands) fall on or near the C_s distortion coordinate and Table VII lists the structural parameters described above for representative complexes (A-H) with N and O donor ligands along this coordinate.

In order to correlate the spectral features of the tyrosinase half-met carboxylates with those of crystallographically characterized Cu(II) model complexes (Table VII) along the C_s distortion coordinate, Figure 5 presents absorption and EPR data for N donor³³ Cu(II) complexes along the coordinate. The previously noted (Table VI) rhombic g values in C_s symmetry are found (Figure 5B) for complexes between the axial C_{4v} and D_{3h} limits. Comparing this rhombic splitting of model complexes on the coordinate and the rhombic splitting observed for half-met *p*-toluate (Table V), the ligand field of this protein derivative appears to be quite far along the coordinate near the trigonal bipyramidal limiting geometry.

The g values of these cupric complexes can provide insight about changes in covalency along the C_s distortion coordinate. Due to covalent interactions with the ligands, the experimentally observed g values are reduced from those predicted by crystal field theory. This can be simply parameterized by an anisotropic orbital reduction factor³⁴ ($k_i \leq 1.0$; $i = x, y, \text{ and } z$) which in effect lowers the spin-orbit coupling to the excited states and the orbital angular momentum in the ground-state wave function. When standard perturbation expressions³⁵ are used,

$$\text{tetragonal} \quad g_{\parallel} = 2.0023 - \frac{8\lambda k_{\parallel}^2}{E_{x^2-y^2} - E_{xz,yz}}$$

$$g_{\perp} = 2.0023 - \frac{2\lambda k_{\perp}^2}{E_{x^2-y^2} - E_{xy}}$$

$$\text{trigonal bipyramidal} \quad g_{\parallel} = 2.0023$$

$$g_{\perp} = 2.0023 - \frac{6\lambda k_{\perp}^2}{E_{x^2} - E_{xz,yz}}$$

(33) We limit this spectral correlation to complexes of one ligand donor type in order to minimize differences in the ligand field strengths; a large set of model complexes along the C_s coordinate have N donor ligands, and we have chosen members of this set with firm spectral assignments for Figure 5.

(34) Gerloch, M.; Miller, J. R. *Prog. Inorg. Chem.* **1968**, *10*, 1-47.

(35) McGarvey, B. R. In "Transition Metal Chemistry"; Carlin, R. L., Ed.; Marcel Dekker: New York, 1968; pp 89-201.

(32) The tilt angle between Cu- L_1 and the normal to the L_3 , L_4 , and L_5 plane is an easily conceptualized C_s distortion parameter; however, it is often difficult in somewhat distorted model complexes to determine the normal to this plane and thus the tilt angle.

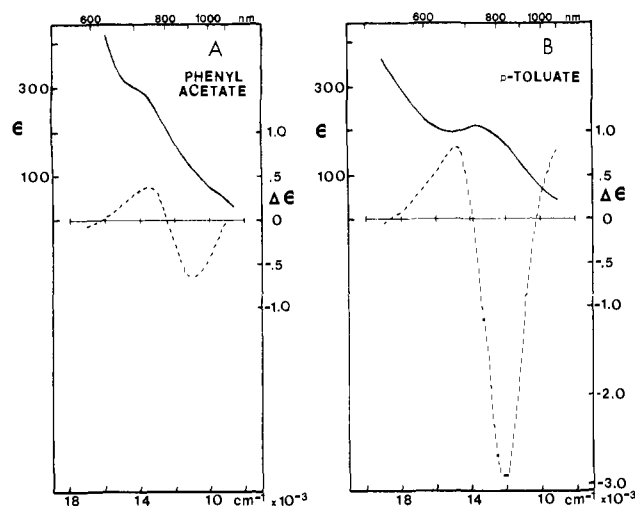


Figure 6. Room temperature absorption (—) and CD (---) spectra for (A) half-met phenylacetate and (B) half-mettyrosinase *p*-toluate; the residual half-met nitrite spectra have been subtracted.

these orbital reduction factors have been calculated for the model complexes in the tetragonal (Figure 5, complex 1: $k_{\parallel}^2 = 0.51$ and $k_{\perp}^2 = 0.49$) and trigonal bipyramidal (Figure 5, complex 5: $k_{\perp}^2 = 0.54$) limits.³⁶ It is found that when the ligand set remains relatively constant, the orbital reduction factors are very similar for the two limits of the C_s distortion coordinate.

In order to describe the ground-state wave function and ligand field excited states along the C_s distortion, we maintain a coordinate system fixed in the tetragonal ($d_{x^2-y^2}$ ground state) limit (Figure 4). The mirror plane therefore contains the y and z axes, and the C_s ground-state wave function therefore is $\Psi(\text{gs}) = ad_{x^2-y^2} + bd_{z^2} + cd_{yz}$ where $a^2 + b^2 + c^2 = 1$. At the other limit of this distortion, the C_3 axis of the trigonal bipyramid is now along x , and thus the D_{3h} ground state is designated as d_{x^2} . However, by maintaining a d orbital basis set also fixed at the tetragonal limit, d_{x^2} corresponds to 75% $d_{x^2-y^2}$ + 25% d_{z^2} . It should be noted that in the more common coordinate system, C_3 is along z , leading to a d_{z^2} ground state in D_{3h} symmetry. When the fixed coordinate system of Figure 4 and the d orbital basis set of the tetragonal limit are used, the ligand field transition energies obtained from the optical absorption spectra are designated by the dominant tetragonal d orbital contribution to the associated excited-state wave function.

Figure 5A shows the ligand field transition energies for the N donor model complexes along the C_s distortion coordinate. The total ligand field absorption envelope shows no dramatic shift; however, the individual $d-d$ transition energies can be strongly perturbed by this structural distortion. While three of the transition energies show small changes between the limiting structural geometries, the $\Psi(d_{yz}) \leftarrow \Psi(\text{gs})$ transition dramatically shifts to lower energy, empirically falling even below the $\Psi(d_{z^2}) \leftarrow \Psi(\text{gs})$ transition near the trigonal bipyramidal limit. Thus, the low energy of this transition is diagnostic for this region of the distortion coordinate.

Figure 6A shows the room temperature ligand field absorption and CD spectra for phenylacetate half-mettyrosinase. Tetragonal cupric complexes generally have most of their $d-d$ absorption intensity associated³⁷ with the ${}^2E(d_{xz}, d_{yz}) \leftarrow {}^2B_1(d_{x^2-y^2})$ transition; the ${}^2A_1(d_{z^2}) \leftarrow {}^2B_1(d_{x^2-y^2})$ transition is sometimes observed as a low-energy shoulder. CD spectra of chiral tetragonal Cu(II) complexes and associated calculations³⁸ show that most of the total magnetic dipole character of the ligand field transitions is asso-

(36) In the intermediate lower symmetries, expressions for the orbital reduction factors involve more parameters due to the mixed ground-state and excited-state wave functions.

(37) Hathaway, B. J.; Billing, D. E. *Coord. Chem. Rev.* **1970**, *5*, 143-207.

(38) (a) Strickland, R. W.; Richardson, F. S. *J. Phys. Chem.* **1976**, *80*, 164-173. (b) Yeh, C.-Y.; Richardson, F. S. *Inorg. Chem.* **1976**, *15*, 682-690.

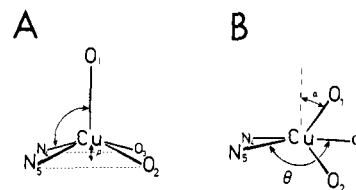


Figure 7. Structural representations of the effective (A) tetragonal and (B) C_s distorted half-mettyrosinase copper(II) site.

ciated with the ${}^2E(d_{xz}, d_{yz}) \leftarrow {}^2B_1(d_{x^2-y^2})$ and, in particular, the ${}^2B_2(d_{xy}) \leftarrow {}^2B_1(d_{x^2-y^2})$ transition. Therefore, reasonable spectral assignments³⁹ are the 13 500- cm^{-1} CD peak and the absorption peak maximum ($|\Delta\epsilon/\epsilon| = 0.006$) as ${}^2E(d_{xz}, d_{yz}) \leftarrow {}^2B_1(d_{x^2-y^2})$ and the 11 000- cm^{-1} CD peak ($|\Delta\epsilon/\epsilon| = 0.025$) as ${}^2B_2(d_{xy}) \leftarrow {}^2B_1(d_{x^2-y^2})$. The ${}^2A_1(d_{z^2}) \leftarrow {}^2B_1(d_{x^2-y^2})$ transition is apparently not observed in the room-temperature absorption or CD spectra at energies $>9000\text{ cm}^{-1}$.

Figure 6B shows the analogous spectra for *p*-toluate half-mettyrosinase. Compared to the phenylacetate spectrum, the two dominant CD peaks show only small shifts to higher energy (14 500 and 12 200 cm^{-1}). The Kuhn anisotropy factors ($|\Delta\epsilon/\epsilon|$)⁴¹ for these transitions do not change significantly (~ 0.016 and ~ 0.026 , respectively), indicating that the increase in CD intensity can be attributed to the general increase in ligand field absorption intensity seen for half-met *p*-toluate. The major spectroscopic difference, however, is the appearance of a new positive transition in the half-met *p*-toluate CD spectrum at an energy $<10000\text{ cm}^{-1}$ ($|\Delta\epsilon/\epsilon| > 0.025$ at 9000 cm^{-1}). Apparently one ligand field transition has shifted to lower energy consistent with the behavior of the $\Psi(d_{yz}) \leftarrow \Psi(\text{gs})$ transition of the N donor model complexes near the trigonal bipyramidal limit seen in Figure 5A. Thus, both the rhombic splitting of the EPR spectrum and the relative energies of the $d-d$ transitions of half-met *p*-toluate indicate that the Cu(II) coordination is strongly distorted toward a trigonal bipyramidal geometry.

In order to quantify the position of half-met *p*-toluate on the C_s distortion coordinate and determine the half-met ground-state wave functions, we have performed a ligand field analysis of the C_s distortion coordinate by using an N and O ligand donor set appropriate for the half-mettyrosinase site. The initial requirements for the tetragonal half-met ligand field are based on the spectroscopically effective active site (Figure 7A) and include two strongly bound cis equatorial imidazole (N4, N5) ligands, two strongly bound cis equatorial oxygen donor ligands (O3 from the endogenous bridge (RO⁻) and O2 from exogenous carboxylate), and a weakly bound axial O1 donor ligand (exchangeable H₂O). Structural parameters (Figure 7B) for ligand field calculations along the C_s coordinate follow those observed for model complexes on this coordinate (Table VII).

In this calculation, based on the method of Companion and Komarynsky⁴² as outlined by Penfield et al.,⁴³ we use a fixed tetragonal coordinate system (Figure 4), and the ligand field is introduced as a perturbation on the real d -orbital basis set (ψ_p, ψ_q where $p, q = d_{x^2-y^2}, d_{z^2}, d_{xz}, d_{yz},$ or d_{xy}). A secular determinant $\mathcal{H}_{pq} = \delta_{pq}E_0$ is set up to quantify the splitting and mixing of the

(39) An analogous assignment can be made for half-methemocyanin acetate (*Busycon canaliculatum*): a CD peak at 14 000 cm^{-1} ($=+0.5$) is closely associated with the absorption maximum at 13 800 cm^{-1} and assigned as the ${}^2E(d_{xz}, d_{yz}) \leftarrow {}^2B_1(d_{x^2-y^2})$ transition, a shoulder on the low-temperature absorption envelope (see ref 40) at 11 200 cm^{-1} is assigned as the ${}^2A_1(d_{z^2}) \leftarrow {}^2B_1(d_{x^2-y^2})$ transition, and a CD peak at 10 000 cm^{-1} ($=-0.2$) is assigned as the ${}^2B_2(d_{xy}) \leftarrow {}^2B_1(d_{x^2-y^2})$.

(40) Himmelwright, R. S.; Eickman, N. C.; Solomon, E. I. *Biochem. Biophys. Res. Commun.* **1978**, *81*, 237-242.

(41) Gillard, R. D. In "Physical Methods in Advanced Inorganic Chemistry"; Hill, H. A. O., Day, P., Eds.; Interscience: London, 1968; Chapter 5.

(42) Companion, A. L.; Komarynsky *J. Chem. Educ.* **1964**, *41*, 257-262.

(43) Penfield, K. W.; Gay, R. R.; Himmelwright, R. S.; Eickman, N. C.; Norris, V. A.; Freeman, H. C.; Solomon, E. I. *J. Am. Chem. Soc.* **1981**, *103*, 4382-4388.

Table VIII. Ligand Field Parameters Determined for Structurally Defined Cu(II) Complexes

Cu-O or Cu-N length ^a	O or N ligand	complex ^b	α_2, cm^{-1}	α_4, cm^{-1}
2.36	H ₂ O	A	1 000	950
2.18	formate	B	1 600	2 200
2.16	H ₂ O	C	3 000	3 000
2.13	ether	C	3 500	3 500
2.07	carboxylate	D	8 000	5 200
2.02	H ₂ O	B	7 100	6 000
2.00	formate	A	6 650	6 750
1.97	formate	B	7 000	6 700
1.97	H ₂ O	E	7 300	7 000
1.96	carboxylate	E	7 800	7 800
1.93	carboxylate	C	9 800	9 000
1.92	acac	F	8 450	9 350
1.91	acac	G	9 500	9 500
1.90	acac	H	11 750	10 500
2.05	imidazole	J	11 000	7 000
2.01	imidazole	J, K	12 000	7 500

^aVery little range is found for equatorial Cu-N(imidazole) bond lengths, and 2.01–2.05 roughly spans this range. ^bThe complexes are as follows: (a) [Cu(HCO₂)₂]₄(H₂O) (Kiryama, R.; Ibamoto, H.; Matsuo, K. *Acta Crystallogr.* **1954**, *7*, 482–483), (Billing, D. E.; Hathaway, B. J. *J. Chem. Soc. A* **1968**, 1516–1519); (B) Ba₂[Cu(HCO₂)₆]₄(H₂O) (Sundara Rao, R. V. G.; Sundaramma, K.; Sivankara Rao, G. Z. *Krist.* **1958**, *110*, 231) (Billing, D. E.; Hathaway, B. J. *Z. Krist.* **1958**, *110*, 231); (C) [Cu(CH₃OCH₂CO₂)₂(H₂O)₂] (Prout, C. K.; Armstrong, R. A.; Carruthers, J. R.; Forrest, G. E.; Murray-Rust, P.; Rossotti, F. J. C. *J. Chem. Soc. A*, **1968**, 2791–2813) (Bew, M. J.; Billing, D. E.; Dudley, R. J.; Hathaway, B. J. *J. Chem. Soc. A* **1970**, 2640–2644); (D) [Cu(NH₃)₂(CH₃CO₂)₂] (Davey, G.; Dudley, R. J.; Hathaway, B. J. *J. Chem. Soc. A*, **1971**, 1446–1450); (E) [Cu(Ac-ala)₂]₂(H₂O) (Battaglia, Bonamartini Coradi, A.; Marcotrigiano, G.; Menabue, L.; Pellacani, G. C. *Inorg. Chem.* **20**, **1981**, 1075–1080); (F) [Cu(acac)₂] Ferguson, J. J. *Chem. Phys.* **1961**, *34*, 1609–1613); (G) [Cu(3-Meacac)₂] (Roberts, I.; Truter, M. R. *J. Chem. Soc. A* **1967**, 309–313) (Hathaway, B. J.; Billing D. E.; Dudley, R. J. *J. Chem. Soc. A* **1970**, 1420–1424); (H) [Cu(3-Phacac)₂] (Carmichael, J. W., Jr.; Steinrauf, L. K.; Belford, R. L. *J. Chem. Phys.* **1965**, *43*, 3959–3966) (Belford, R. L.; Carmichael, J. W., Jr. *J. Chem. Phys.* **1967**, *46*, 4515–4522); (J) [Cu(imid)₆](NO₃)₂ (McFadden, D. L.; McPhail, A. T.; Garner, C. D.; Mabbs, F. E. *J. Chem. Soc., Dalton Trans.* **1975**, 263–268); (K) [Cu(imid)₄(NO₃)₂] (McFadden, D. L.; McPhail, A. T.; Garner, C. D.; Mabbs, F. E. *J. Chem. Soc., Dalton Trans.* **1976**, 47–52).

d orbitals by this perturbation. A general form of the elements of this Hamiltonian matrix is

$$\mathcal{H}_{pq} = \langle \psi_p | H | \psi_q \rangle = \sum_{L=1}^N [f(\theta_L, \phi_L) \alpha_2(L, R_L) + g(\theta_L, \phi_L) \alpha_4(L, R_L)]$$

where the sum runs overall N ligands (N = 5 in our calculation). Input parameters for this calculation are (1) the ligand angular coordinates θ_L and ϕ_L , used to calculate f and g (functional forms given in Tables I and II of ref 42) which relate to the integral over the d orbitals of the angular part of the crystal field potential, and (2) the radial integrals which cannot be accurately calculated and thus are included by the empirically determined α_2 and α_4 ligand field parameters that depend on ligand type and Cu–L distance (R_L). We have obtained a set of α_2 's and α_4 's for O donor ligands and imidazole over a range of distances by performing this ligand field calculation for a number of structurally known Cu(II) complexes with these ligands until α_2, α_4 sets were found which provided good matches between the experimental and calculated ligand field transitions. Table VIII lists this set of ligand field parameters which were used as input for the radial terms. After all the terms of the Hamiltonian matrix for a given ligand field have been calculated and summed, the matrix is diagonalized. The resulting output of the calculation is the five d energy levels (eigenvalues: E_m) and the wave function of each level (eigenvectors: $\Psi_m = \sum_p A_{mp} \psi_p$ where $m = 1-5$) for the ligand field. These d energy levels and wave functions are then used to calculate the g values associated with the ligand field, using the general

Table IX. Structural Parameters of Best Fit Ligand Field Calculations

	A. half-met phenylacetate	B. half-met <i>p</i> -toluate
O ₃ -Cu-N ₅	158° ± 4	178° ± 2
O ₂ -Cu-N ₄	158° ± 4	127° ± 7
N ₄ -Cu-O ₁	101° ± 2	117° ± 3
O ₁ -Cu-O ₂	101° ± 2 = 0.38 ± 0.07 Å	113° ± 7 = 27° ± 3
Cu-O ₁	2.16 ± 0.05 Å	2.00 ± 0.03 Å
Cu-O ₂	1.97 ± 0.03 Å	1.96 ± 0.03 Å
Cu-O ₃	1.97 ± 0.03 Å	1.92 ± 0.03 Å
Cu-N ₄	2.01 ± 0.03 Å	2.05 ± 0.03 Å
Cu-N ₅	2.01 ± 0.03 Å	2.01 ± 0.03 Å
$\rho = 0.38 \pm 0.07 \text{ \AA}$		$\alpha = 27 \pm 3^\circ$

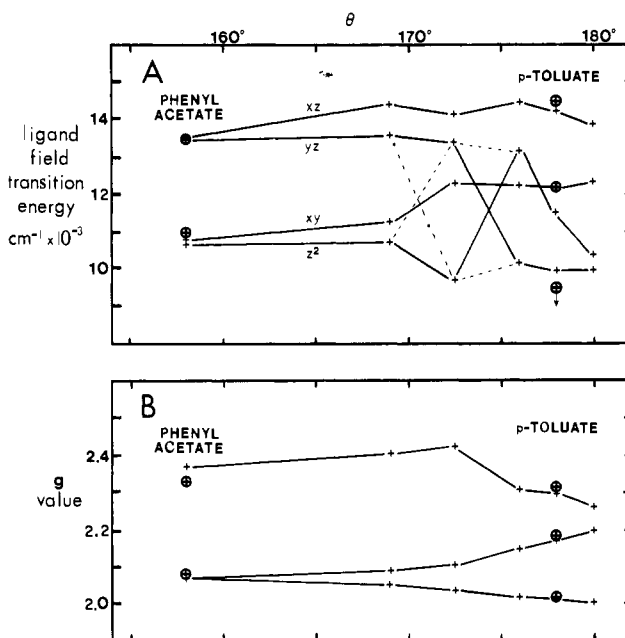


Figure 8. Calculated ligand field transition energies (A) and g values (B) (reduced by an orbital reduction factor $k^2 = 0.605$) for effective half-mettyrosinase ligand fields distorted along the C_z coordinate defined by the O₃-Cu-N₅ angle (θ).

perturbation expression for the g_{ij} ($i, j = x, y, \text{ and } z$; coordinate system of Figure 4) tensor elements

$$g_{ij} = 2 \left(\delta_{ij} - \lambda \sum_{m=2}^5 \frac{\langle \psi_1 | L_i | \psi_m \rangle \langle \psi_m | L_j | \psi_1 \rangle}{(E_m - E_1)} \right)$$

where $m = 1$ is the ground state and $\lambda_{\text{Cu(II)}} = -830 \text{ cm}^{-1}$. Diagonalizing this tensor gives the principal g values which, after including orbital reduction parameters (k_i^2) to account for covalency, can be compared to the experimental values.

Ligand field calculations for phenylacetate half-mettyrosinase were performed until the calculated d energy levels gave (1) a close match of the experimental and calculated ligand field transition energies and (2) calculated g values with no rhombic splitting. As mentioned previously, there is a direct correlation between the length of the Cu–L(axial) bond and the displacement of the copper from the equatorial plane (ρ in Figure 7A) in five-coordinate square-pyramidal cupric complexes. Since the axial bond is the dominant perturbation along the tetragonal z axis, interaction of the axial ligand with the Cu(II) will determine the energy of the ${}^2A_1(d_{z^2}) \leftarrow {}^2B_1(d_{x^2-y^2})$ transition. Displacement of the copper from the equatorial plane, however, will modify the equatorial ligand field interaction which will be reflected in the energies and splitting of the ${}^2E(d_{xz}, d_{yz}) \leftarrow {}^2B_1(d_{x^2-y^2})$ and ${}^2B_2(d_{xy}) \leftarrow {}^2B_1(d_{x^2-y^2})$ transitions. As the ${}^2A_1(d_{z^2}) \leftarrow {}^2B_1(d_{x^2-y^2})$ transition is not observed for half-met phenylacetate, the energies and splitting (2400 cm^{-1}) of the ${}^2E(d_{xz}, d_{yz}) \leftarrow {}^2B_1(d_{x^2-y^2})$ and ${}^2B_2(d_{xy}) \leftarrow {}^2B_1(d_{x^2-y^2})$ transitions have been used to determine these coupled structural parameters of the ligand field.

Table X. Calculated Best Fit EPR Hyperfine Coefficients and Calculated Hyperfine Parameters

A. half-met phenylacetate			B. half-met <i>p</i> -toluate		
$\alpha^2 = 0.86$	$a^a = 1.0$		$\alpha^2 = 0.85$	$a^a = 0.952^b$	
$\kappa^2 = 0.31$	$b^a = 0.0$		$\kappa^2 = 0.21$	$b^a = 0.306^b$	
	calcd	exptl		calcd	exptl
A_1	-1	0 ± 5	A_1	76	83 ± 6
A_2	-1	0 ± 5	A_2	-20	22 ± 4
A_3	-157	158 ± 2	A_3	-94	90 ± 2

^a Ground-state wave function coefficients for the $d_{x^2-y^2}$ (a) and d_{z^2} (b) orbitals. ^b These ground-state wave function coefficients are for the calculated ligand field at 176° on the C_s distortion coordinate.

Table IXA lists the structural features (see Figure 7A) of the ligand field which provide the best fit for half-met phenylacetate, and the left side of Figure 8A compares the observed (\oplus) and calculated (+) ligand field transition energies. The equatorial Cu-O and Cu-N distances of the best fit ligand field are consistent with EXAFS results⁴⁴ for oxy- and mettyrosinase. The low energies of the ${}^2E \leftarrow {}^2B_1$ and ${}^2B_2 \leftarrow {}^2B_1$ transitions and the splitting between them (2400 cm^{-1}), however, require displacing the copper $\sim 0.38 \text{ \AA}$ out of the equatorial N_2O_2 plane which, in turn, correlates with the rather short $2.16\text{-}\text{\AA}$ Cu-O(axial) distance. This distance seems small for an axial exchangeable water and is apparently not necessary to give a good fit⁴⁴ of the EXAFS spectra. If the energy of the ${}^2A_1 \leftarrow {}^2B_1$ transition was observed, it would provide a direct means of calibrating the Cu-O(axial) distance (the best fit calculation places the ${}^2A_1 \leftarrow {}^2B_1$ transition nearly coincident with the ${}^2B_2 \leftarrow {}^2B_1$ transition at $\sim 11\,000 \text{ cm}^{-1}$). The Cu-O(axial) distance, however, therefore, has a higher degree of uncertainty in this calculated ligand field of half-mettyrosinase phenylacetate. Ligand field absorption and CD data for half-metmetocyanin acetate³⁹ show all three tetragonal d-d bands; an analogous calculation for this derivative gives a $\sim 2.2\text{-}\text{\AA}$ Cu-O(axial) distance and the copper displaced $\sim 0.32 \text{ \AA}$ above the equatorial N_2O_2 plane (these structural parameters are very similar to those found for $[\text{Cu}(\text{cyclo-ps})(\text{H}_2\text{O})](\text{ClO}_4)^{45}$).

The g values have been calculated for the phenylacetate half-mettyrosinase ligand field, and the orbital reduction parameters required to fit the experimentally observed g values are $k_{\parallel}^2 = 0.54$ and $k_{\perp}^2 = 0.67$. As has been noted, the orbital reduction factors for a consistent ligand set are not significantly different near the two limits of the C_s coordinate; thus, the average of these values ($k_{\text{av}}^2 = 0.605$) is used to generally account for covalency in the following calculations of half-mettyrosinase spectral features. When this k_{av}^2 value is used; reasonable agreement with the experimental (\oplus) g values (Figure 8B, left side) is obtained.

Ligand field calculations for five-coordinate Cu(II) geometries along the C_s distortion coordinate, beginning with the best fit half-met phenylacetate ligand field, have been performed. Because this is a complicated distortion coordinate, the structural parameters from model complexes on this coordinate (see Table VII) have been used to calibrate and quantify the earlier indicated changes in bond lengths and angles along the calculated C_s coordinate. Even though the 180° limit is structurally very close to a trigonal bipyramid, this does not correspond to pure D_{3h} symmetry because of the different ligand types and their associated ligand field strengths; the ground-state wave function at this limit of the calculated C_s coordinate is $\sim 75\%$ of the way to axial D_{3h} symmetry.

Figure 8 shows the calculated d-d transition energies and g values for ligand fields along the C_s distortion coordinate. The solid lines in Figure 8A follow the dominant tetragonal d orbital character of the ligand field transitions, while the dashed lines indicate significant mixing between d_{yz} and d_{z^2} in the $170\text{-}175^\circ$ region. Comparing the experimental d-d transitions and g values

of half-met *p*-toluate (\oplus) (right side of Figure 8) to the calculation results places the half-met *p*-toluate ligand field at $178 \pm 2^\circ$ along the coordinate. The structural parameters of this ligand field are listed in Table IXB (see Figure 7B) and show that it is close to a trigonal bipyramidal geometry.

The results of this ligand field calculation provide a reasonable assignment⁴⁶ for the ligand field spectrum (Figure 6B) of half-met *p*-toluate in C_s effective symmetry. The $14\,500\text{-cm}^{-1}$ CD peak is assigned as ${}^2A''(d_{xz}) \leftarrow {}^2A'(gs)$ and the $12\,200\text{-cm}^{-1}$ CD peak as ${}^2A''(d_{xy}) \leftarrow {}^2A'(gs)$. The $<10\,000\text{-cm}^{-1}$ CD feature, which was one of the major criterion requiring this $\sim 178^\circ$ ligand field geometry, is assigned as ${}^2A'(d_{yz}) \leftarrow {}^2A'(gs)$. The ${}^2A'(d_{z^2}) \leftarrow {}^2A'(gs)$ transition is apparently not observed; however, the best fit calculated ligand field places this transition at $\sim 11\,500 \text{ cm}^{-1}$.

The calculated rhombic g values along the C_s coordinate are another major criterion requiring the $\sim 178^\circ$ distortion for *p*-toluate half-mettyrosinase. The ground-state wave function which is associated with this best fit ligand field is quantitatively found to be $\Psi(gs) = 0.926(\pm 0.026)d_{x^2-y^2} + 0.373(\pm 0.067)d_{z^2} - 0.077(\pm 0.077)d_{yz}$. The large experimentally observed rhombic splitting⁴⁷ for this derivative, therefore, is found to be due to significant d_{z^2} mixing⁴⁸ into the ground-state wave function near the trigonal bipyramidal geometry and the large energy splitting of the dominantly d_{xz} and d_{yz} levels.

When standard expressions³⁵ for nuclear hyperfine coupling

$$A_1 = P_d[-\kappa + \alpha^2 2(a^2 - b^2)/7 + \alpha^2 4ab(3)^{1/2}/7 + (g_1 - 2.0023) - (3a - (3)^{1/2}b)(g_2 - 2.0023)/14(a + (3)^{1/2}b) - b(g_3 - 2.0023)/7a]$$

$$A_2 = P_d[-\kappa + \alpha^2 2(a^2 - b^2)/7 - \alpha^2 4ab(3)^{1/2}/7 + (g_2 - 2.0023) - (3a + (3)^{1/2}b)(g_1 - 2.0023)/14(a - (3)^{1/2}b) + b(g_3 - 2.0023)/7a]$$

$$A_3 = P_d[-\kappa - \alpha^2 4(a^2 - b^2)/7 + (3a - (3)^{1/2}b) \times (g_2 - 2.0023)/14(a + (3)^{1/2}b) + (3a + (3)^{1/2}b)(g_1 - 2.0023)/14(a - (3)^{1/2}b) + (g_3 - 2.0023)]$$

and the experimental g values and the ground-state wave function coefficients (a , b) of the best fit ligand fields were used, the hyperfine coupling parameters were calculated for half-met phenylacetate and half-met *p*-toluate (Table X). The α^2 (percent metal character in the ground-state wave function, reduced from 1.0 due to covalent electron delocalization into the ligand orbitals) and κ (Fermi contact or s orbital contribution) parameters were systematically varied until the best fit to the experimental $|A|$ values was achieved (P_d was fixed at $360 \times 10^{-4} \text{ cm}^{-1}$). For half-met phenylacetate, α^2 and κ are typical of tetragonal Cu(II) complexes with fairly hard N and O donor ligands. For half-met *p*-toluate, there is no change in covalency as indicated by α^2 ;

(46) The ligand field assignment emphasizes CD spectral features as the absorption d-d bands are not resolved. To further evaluate this assignment, the real d orbital coefficients of the ligand field energy levels along the C_s coordinate (Figure 8A) have been used to determine the matrix elements of the angular momentum operator connecting the ground and excited states $\langle \psi_1 | L | \psi_M \rangle$. These matrix elements indicate the upper limit of the relative CD intensities of the ligand field transitions (the rotatory strength depends on the projection of the electric and magnetic dipoles and is maximal when these dipole moments are colinear). The ${}^2A''(d_{xz}) \leftarrow {}^2A'(gs)$ and ${}^2A''(d_{xy}) \leftarrow {}^2A'(gs)$ transitions retain most of the magnetic dipole character all along the C_s coordinate but the ${}^2A'(d_{yz}) \leftarrow {}^2A'(gs)$ transition carries noticeable magnetic dipole character as it descends to lower energy. While the ${}^2A'(d_{z^2}) \leftarrow {}^2A'(gs)$ transition has some magnetic dipole character along the coordinate, when it has descended to $<11\,000 \text{ cm}^{-1}$, near the trigonal bipyramid, it has lost all magnetic dipole character. Thus, the assignment of the new low-energy CD feature at $<9000 \text{ cm}^{-1}$ as the ${}^2A'(d_{yz}) \leftarrow {}^2A'(gs)$ transition is consistent with its magnetic dipole character.

(47) Hathaway has noted (Billing, D. E.; Dudley, R. J.; Hathaway, B. J.; Tomlinson, A. A. G. *J. Chem. Soc. A* 1971, 691-696) that the empirical parameter $R = (g_2 - g_1)/(g_3 - g_2)$ quantifies the rhombic splitting of the g values and provides some insight into the nature of the ground state ($R < 1.0$ for predominantly $d_{x^2-y^2}$ and $R > 1.0$ for predominantly d_{z^2}); half-met *p*-toluate has $R = 1.54$. This description thus also supports a distorted trigonal bipyramidal ligand field for half-met *p*-toluate.

(48) Hitchman, M. A. *J. Chem. Soc. A* 1970, 4-9.

(44) Woolery, G. L.; Powers, L.; Winkler, M.; Solomon, E. I.; Lerch, K.; Spiro, T. G. *Biochim. Biophys. Acta* 1984, 783, 155-161.

(45) Anderson, O. P.; Packard, A. B. *Inorg. Chem.* 1979, 18, 1940-1947.

however, the Fermi contact term, κ , is significantly reduced. Cu(II) complexes⁴⁹ with dominantly d_{z^2} ground states have quite small Fermi contact terms apparently due to symmetry-allowed 4s mixing⁵⁰ into the ground state; the reduced κ value required for half-met *p*-toluate can reasonably be associated with a small amount of 4s mixing. The large hyperfine coupling parameters associated with g_x and g_y of half-met *p*-toluate, therefore, are seen to dominantly arise from direct and indirect effects of d_{z^2} mixing into the ground-state wave function in the distorted trigonal bipyramidal ligand field. Finally, both the orbital reduction factor k_{ov} (0.78), used in determining the ligand field g values, and the electron delocalization parameter α^2 (0.85), used in calculating the hyperfine coupling, qualitatively reflect a similar magnitude of covalency which does not change significantly between phenylacetate and *p*-toluate. Therefore, in the half-mettyrosinase site, comparable substrate analogue bonding interaction with the copper(II) is found to be similar when poor competitive inhibitors bind in a tetragonal geometry and good competitive inhibitors bind in a distorted trigonal bipyramidal geometry.

Discussion

As demonstrated by kinetic, equilibrium, and spectroscopic studies, the interactions of substrates and inhibitors with tyrosinase take place at the binuclear copper center, which is the active site of catalysis.

With regard to their ability to bind to the site, competitive inhibitors can be divided into two groups: (1) poor inhibitors, which show an equilibrium constant for binding to the enzyme similar to that for binding to aqueous Cu(II) complexes, and (2) good inhibitors, which are substrate analogues in that the carboxylate is conjugated into the aromatic ring, producing a planar structure, and which bind with an equilibrium constant higher by an order of magnitude relative to aqueous Cu(II). Thus, it appears that the protein pocket surrounding the copper site contributes to the stabilization of substrate (analogue) binding to the active site. Associated with this increased stability are unusual Cu(II) spectral features which are related to a difference in the geometry of substrate binding to the copper site.

The poor inhibitors produce EPR, absorption, and CD spectral features typical of normal tetragonal Cu(II). These reflect the ground-state wave function and the energies of the d orbitals. A ligand field analysis of these spectral features, calibrated from tetragonal model complexes with nitrogen and oxygen ligation, yields a confirmation of spectral assignments and allows us to estimate the geometry of this copper site. The relatively low energy of the ligand field transitions and small splittings of the ${}^2E \leftarrow {}^2B_1$ and ${}^2B_2 \leftarrow {}^2B_1$ transitions requires the tetragonal site to be distorted toward square pyramidal with the copper displaced from the equatorial plane by ~ 0.3 Å toward the axial ligand.

Alternatively, the unusual spectral features associated with the good competitive inhibitors (*p*-toluate, etc.) binding to the copper site (large rhombic splitting in the g_{\perp} region, large hyperfine splitting of the lowest g value, and a low-energy ($<10\,000$ cm^{-1}) transition in the CD spectrum) result from a significant distortion of the Cu(II) site toward a trigonal bipyramidal geometry along the C_2 distortion coordinate.

Thus, the protein pocket appears to contribute to the stabilization of substrate analogue binding in a geometry which is at an intermediate position along the reaction coordinate for associative ligand displacement. A simple reaction coordinate diagram for associative ligand substitution in the absence of the protein is pictured as a solid line in Figure 9. Inclusion of the substrate interaction with the protein pocket results in stabilization of the substrate midway along this coordinate, producing the dotted line in Figure 9. Thus, the activation barrier for the rearrangement is lowered by the protein-ligand interaction, with the ligand "on" rate being preferentially increased. This substrate-protein interaction will clearly assist in the catalytic hydroxylation reaction presented in Figure 1. Both the rate of reaction will be increased

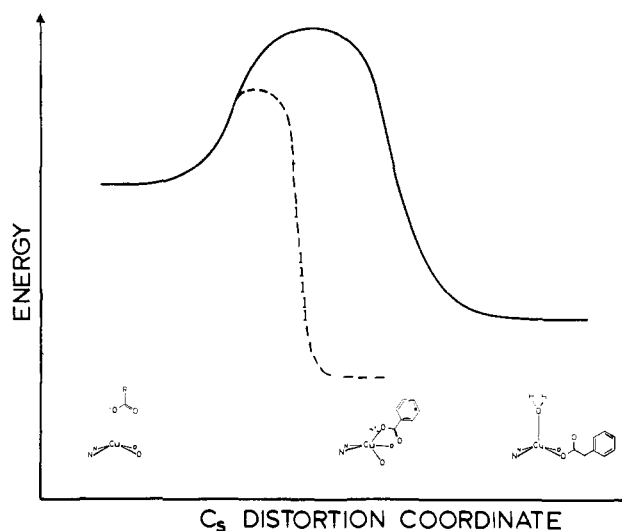


Figure 9. Reaction coordinate diagram for associative ligand substitution in the copper site of tyrosinase. The solid line corresponds to ligand binding in the absence of ligand-protein interaction (phenylacetic acid). The dotted line corresponds to binding when the side chain of the ligand interacts with the protein pocket (*p*-toluic acid). The structures (bottom) represent species present at the different points in the C_2 reaction coordinate.

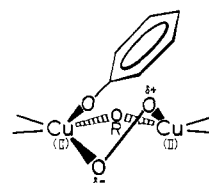


Figure 10. Structural mechanism for the hydroxylation of monophenolic substrates by oxytyrosinase.

and the substrate will be positioned in a geometry suited to chemical attack at the ortho aromatic position by the peroxo oxygen atom bound at the adjacent copper (Figure 10). Furthermore, this peroxide, initially forming an unpolarized μ -1,2 bridge between equatorial positions of the Cu(II) ions, is labilized by this rearrangement of the copper coordination geometry, introducing some polarization into the O-O bond and activating the reaction with substrate.

The possible electronic pathways available for the ortho-hydroxylation reaction in the ternary complex pictured in Figure 10 fall under the categories of homolytic and heterolytic attack, with the latter comprising nucleophilic-, electrophilic-, and oxonium-type reactions.

A pathway relying on homolysis of peroxide would parallel the Fenton-type chemistry usually observed for copper-catalyzed oxidations in aqueous solutions.⁵¹ However, for the ternary substrate oxy site, this would require a one-electron oxidation of the bound phenolic substrate in order to generate a hydroxyl radical. This reaction does not appear to be thermodynamically accessible. If we assume the midpoint potentials of the phenolate and peroxide bound to the metals to be similar to those of the protonated forms of this molecule, we can compare measurements done at pH 0, where both species are fully protonated. $E_{1/2}$ for the phenoxonium/phenol couple is 1.1 V,⁵² compared with a value of less than 0.91 V for the $\text{H}_2\text{O}_2/\text{H}_2\text{O}$, HO \cdot couple.⁵³ Furthermore, it appears that a necessary step in the one-electron

(51) Sheldon, R. A.; Kochi, J. K. "Metal-Catalyzed Oxidations of Organic Compounds"; Academic Press: New York, 1981; pp 34-68.

(52) Ronlan, A. In "Encyclopedia of Electrochemistry of the Elements"; Bard, A. J., Lund, H., Eds.; Marcel Dekker: New York, 1978; Vol. XI, pp 242-267.

(53) Sawyer, D. T.; Nanni, E. J.; Roberts, J. L., Jr. In "Electrochemical and Spectrochemical Studies of Biological Redox Components"; Kadish, K. M., Ed.; American Chemical Society: Washington, DC, 1982; *Adv. Chem. Ser. No. 201*, pp 585-600.

(49) Hagen, S. H.; Trappeniers, N. J. *Physica* **1970**, *47*, 165-181.

(50) Griffith, J. S. *Disc. Faraday Soc.* **1958**, *26*, 81-86.

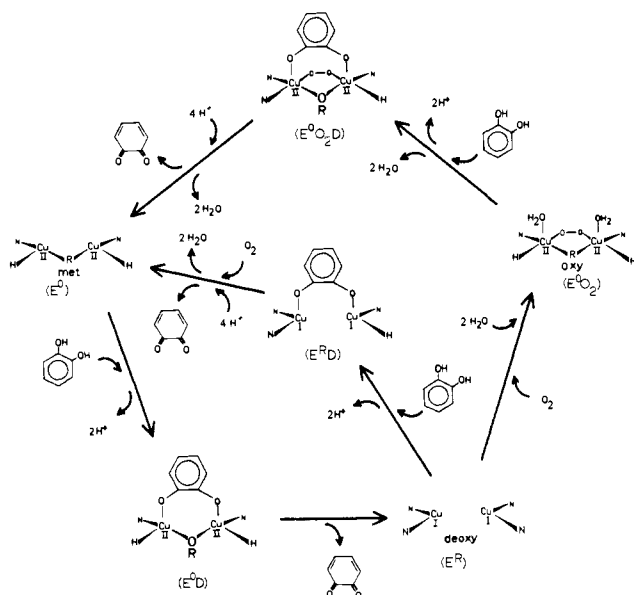


Figure 11. Catalytic cycle for oxidation for diphenolic substrate to *o*-quinones by tyrosinase in the presence of O₂.

oxidation of monophenols is deprotonation concomitant with electron transfer.⁵² This would lead to dissociation of the extremely reactive monophenolic radical from the copper site. Instead it seems more reasonable that the protein inhibits the possibility of Fenton chemistry in relation to aqueous copper by keeping the peroxide intermediate, produced by the two-electron reduction of dioxygen, tightly bound to the binuclear cupric active site.

Among the heterolytic pathways, nucleophilic attack on the aromatic ring is not a likely possibility, since in the absence of strong electron-withdrawing substituents, aromatic rings show very little propensity toward this type of reactivity.⁵⁴

Alternatively, aromatic systems are highly susceptible to electrophilic substitution. While hydrogen peroxide does not typically show electrophilic behavior, this reactivity mode does occur in the presence of strong acid catalysts.⁵⁵ A detailed calculation of the bonding is required to describe the electronic structure of the ternary complex in Figure 10 and in particular the polarization of the peroxide which is now asymmetrically bound due to the labilization at one copper induced by substrate binding. Calculations of dioxygen terminally bound to Fe porphyrin⁵⁶ indicate that there should be some net positive charge on the oxygen atom bound to the nonlabilized copper, as indicated in Figure 10. This positively polarized oxygen atom is well oriented for hydroxylation at the ortho position of the phenol.

Finally, the possibility of attack on the aromatic ring by an oxonium-copper species in a manner similar to the mechanism

of the monooxygenase cytochrome P-450 proposed by Groves⁵⁷ must be considered. This, however, would require the four-electron oxidation of the coupled binuclear copper active site by the dioxygen. Since dioxygen reacts with deoxytyrosinase to yield a stable [Cu^{II}Cu^{II}] peroxide adduct in oxytyrosinase, formation of oxonium ion would have to be triggered by binding and rearrangement of the substrate in the coordination sphere of the copper. For oxonium formation, this rearrangement would then be required to favor the Cu(III) oxidation state which is known to be stabilized by strongly electron-donating ligands in a square-planar geometry with no axial ligation.⁵⁸ However, our ligand field calculations combined with spectral studies show that the distortion from square-pyramidal to trigonal bipyramidal involves no change in electron delocalization between the ligand and metal orbitals and a loss of only some 15 mV in ligand field stabilization energy of the (+2) oxidation state; an even larger destabilization would be associated with the Cu(III) oxidation state due to its stronger ligand field. Thus, it seems unlikely that the distortion upon substrate binding in Figure 10 could lead to oxonium ion formation.

In summary, the structural and electronic characteristics of the peroxy-substrate-binuclear copper ternary complex in Figure 10 seem to be most compatible with oxidation of monophenol via electrophilic attack by peroxide on the aromatic ring of the substrate.

Finally, kinetic results indicate that the oxidation of diphenol substrates to *o*-quinones by tyrosinase has less geometric and electronic requirements than does monophenol oxidation. Diphenol coordinates to the reduced (deoxy), oxidized (met), and oxygenated (oxy) forms of the binuclear copper active site and is oxidized by the latter two forms. Furthermore, in contrast to monophenol oxidation, bulky substituents do not appear to affect diphenol turnover, indicating that axial-to-equatorial rearrangement at the copper may not be required for a simple two-electron transfer. Thus, the scheme presented in Figure 11 is a reasonable structural representation for the diphenol reactivity at the coupled binuclear copper active site of tyrosinase.

Acknowledgment. We wish to thank Harvey Schugar for useful discussions and acknowledge NIH Grant NIH AM 31450 for support of this research.

Registry No. L-DOPA, 59-92-7; D-DOPA, 5796-17-8; Cu, 7440-50-8; tyrosinase, 9002-10-2; L-tyrosine, 60-18-4; D-tyrosine, 556-02-5; tyramine, 51-67-2; 4-hydroxyphenylacetic acid, 156-38-7; *p*-*tert*-butylphenol, 98-54-4; 3-hydroxytyramine, 51-61-6; 3,4-dihydroxyphenylacetic acid, 102-32-9; *p*-*tert*-butylcatechol, 98-29-3; *o*-toluic acid, 118-90-1; *o*-bromobenzoic acid, 88-65-3; acetic acid, 64-19-7; phenylacetic acid, 103-82-2; naphthylacetic acid, 26445-01-2; cyclohexanecarboxylic acid, 98-89-5; cyclopentanecarboxylic acid, 3400-45-1; *m*-toluic acid, 99-04-7; *m*-bromobenzoic acid, 585-76-2; benzoic acid, 65-85-0; *p*-toluic acid, 99-94-5; *p*-bromobenzoic acid, 586-76-5; *p*-ethylbenzoic acid, 619-64-7; picolinic acid, 98-98-6; terephthalic acid, 100-21-0.

(54) Sykes, P. "A Guidebook to Mechanism in Organic Chemistry", 4th ed.; Longman Group Ltd.: New York, 1975; pp 129-174.

(55) Sheldon, R. A.; Kochi, J. K., ref 51, pp 381-382.

(56) Karplus, M. In "Hemoglobin and Oxygen Binding"; Ho, C., Ed.; Elsevier/North Holland: New York, 1982; pp 3-11.

(57) Groves, J. T.; Van Der Puy, M. *J. Am. Chem. Soc.* **1976**, *98*, 5290-5297.

(58) Margerum, D. W. In "Oxidases and Related Redox Systems"; King, T. E., Mason, H. S., Morrison, M., Eds.; Pergamon Press: Oxford, 1982; pp 193-206.